Nanocrystal Catalysts

DOI: 10.1002/ange.201102578

Atomic-Distribution-Dependent Electrocatalytic Activity of Au–Pd Bimetallic Nanocrystals**

*Jong Wook Hong, Dongheun Kim, Young Wook Lee, Minjung Kim, Shin Wook Kang, and Sang Woo Han**

During the past decade, bimetallic nanocrystals (NCs) with core–shell and alloy structures have attracted tremendous research interest because of their prominent catalytic activities and stabilities over monometallic NCs.[1–5] Several previous studies have shown that the catalytic performance of bimetallic NCs could be tuned through the modulation of their morphology, size, and composition. For example, control over the morphology of NCs can tailor their catalytic activity and selectivity because the surfaces of NCs are enclosed by specific facets according to their shapes, which play a decisive role in determining the overall catalytic properties of the NCs.[6–9] In addition, the variation of NC size should change the relative amount of catalytically active surface area, and this results in the alteration of the catalytic reactivity of NCs.[10–12] Since the relative amount of each constituent metal in the bimetallic NCs could modify the electronic state of the primary catalytic component and tune the binding properties for intermediate species during the reaction, the composition of bimetallic NCs also has a great influence on their catalytic properties.[13–15]

Despite the fact that the atomic distribution in bimetallic NCs could have a significant impact on their catalytic performance, this variable has not been closely explored relative to the extensive studies on the morphology-, size-, and composition-dependent catalytic efficiencies of NCs. This difference can be attributed to certain experimental difficulties. To study the influence of the atomic distribution in bimetallic NCs, NCs with various distributions of constituent metals should be prepared under similar experimental conditions, while the shape and size are maintained. Furthermore, the structure-regulating surfactant must be the same for all NCs for exact comparison because the catalytic properties of NCs are usually affected by the surfactant molecules.[16,17] However, it is an extremely hard task to synthesize atomic-distribution-controlled bimetallic NCs with identical morphology and size together with the same surfactant because of the complex NC growth kinetics of bimetallic systems. In this regard, the preparation of NCs that satisfy these requirements and investigation of their properties would be very intriguing and significant for advanced catalytic applications.

In this work, we synthesized Au–Pd alloy, Au@Pd core–shell, Pd, and Au NCs with an identical octahedral morphology (Figure 1), which is a representative polyhedral structure enclosed by {111} facets, to investigate the effect of atomic distribution in bimetallic NCs on the electrocatalytic performance toward formic acid oxidation. The surface of the Au@Pd bimetallic core–shell NCs consists exclusively of Pd, whereas that of the Au–Pd alloy NCs has Pd and Au compositions simultaneously. The prepared octahedral NCs are of similar size and have the same surfactant, cetyltrimethylammonium (CTA^+), which was used in the synthesis. Since the direct formic acid fuel cell (DFAFC) has drawn increasing attention as an alternative power source for portable electronic devices,[18,19] the electrooxidation of formic acid was chosen as a model catalytic reaction. In addition, Pd and Au were selected as composition ingredients because Pd nanostructures have been reported to have efficient electrocatalytic activity for formic acid oxidation,[20–22] and incorporation of Au into Pd catalysts improves catalytic activity and selectivity and provides resistance to poisoning.[7,23] The catalysis experiments unambiguously demonstrate that the activity and stability of the NCs can be tuned by changing their atomic distributions.

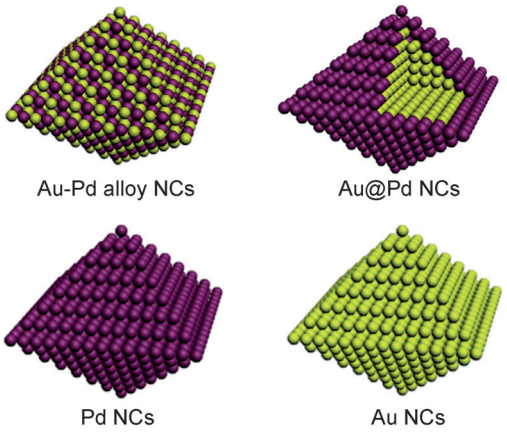

Figure 1. Geometrical models of the octahedral Au–Pd alloy, Au@Pd core–shell, Pd, and Au NCs. Violet and yellow denote Pd and Au, respectively.

[*] J. W. Hong, D. Kim, Y. W. Lee, M. Kim, S. W. Kang, Prof. S. W. Han
Department of Chemistry and KI for the NanoCentury, KAIST
Daejeon 305-701 (Korea)
E-mail: sangwoohan@kaist.ac.kr
Homepage: http://ntl.kaist.ac.kr

[**] This work was supported by Basic Science Research Programs (2008-0062042, 2010-0029149), Future-based Technology Development Program (Nano Fields) (2009-0082640), and Pioneer Research Center Program (2009-0082813) through the National Research Foundation (NRF) funded by the Korean government (MEST).

Supporting information for this article is available on the WWW under http://dx.doi.org/10.1002/anie.201102578.

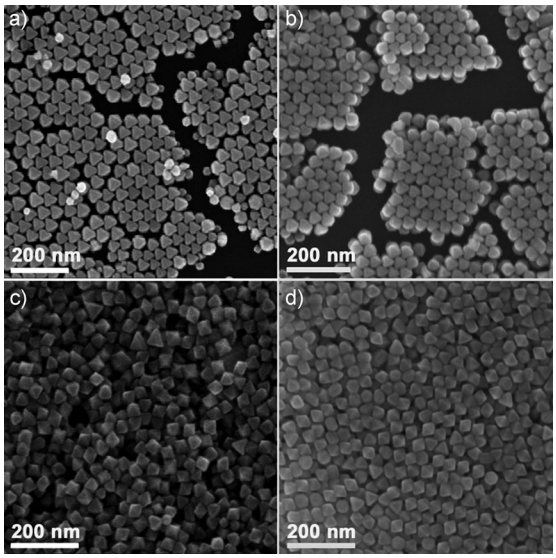

Figure 2. SEM images of a) Au–Pd alloy, (b) Au@Pd core–shell, (c) Pd, and (d) Au NCs.

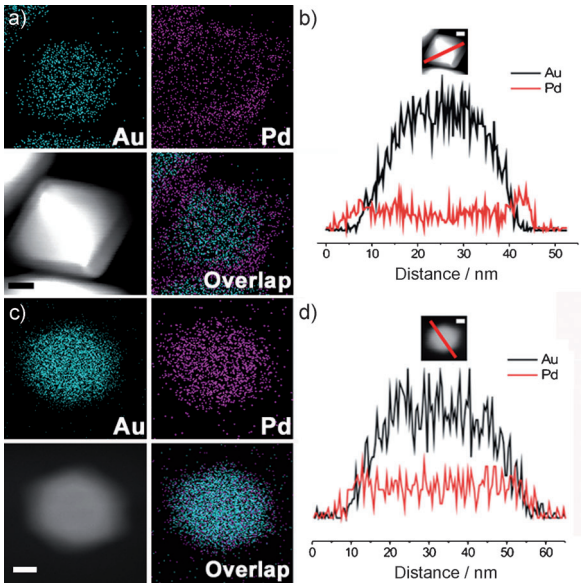

Figure 3. HAADF-STEM-EDS mapping images of an octahedral a) Au@Pd and c) Au–Pd alloy NC. HAADF-STEM image and cross-sectional compositional line profiles of an octahedral b) Au@Pd and d) Au–Pd alloy NC. The scale bars are 10 nm.

NCs with various atomic distributions were synthesized in aqueous solutions by employing the same surfactant (CTA^+) and reducing agent (L-ascorbic acid). Figure 2 shows typical scanning electron microscopy (SEM) images of the as-prepared NCs, indicating that the NC sizes of the various samples are very similar and the NCs definitely have identical octahedral morphology. The average edge lengths of the Au–Pd alloy, Au@Pd core–shell, Pd, and Au NCs are 40 ± 5, 39 ± 3, 38 ± 4, and 34 ± 5 nm, respectively. The Au@Pd core–shell and Au octahedral NCs were prepared by following the reported protocols, which we developed previously.[24,25] The Au/Pd ratio of the Au@Pd core–shell NCs was estimated to be 4:1 by inductively coupled plasma–atomic emission spectrometry (ICP-AES), and the mean thickness of Pd shell was 5 nm. Elemental mapping of Au and Pd, and the cross-sectional compositional line profiles on a single octahedral Au@Pd NC obtained by high-angle annular dark-field scanning transmission electron microscopy (HAADF-STEM)–energy-dispersive X-ray spectroscopy (EDS) demonstrate that the prepared NCs have core–shell structure (Figure 3a,b). In this work, the methods of synthesizing octahedral Au–Pd alloy and Pd NCs were newly developed. In particular, this is the first report on the synthesis of bimetallic alloy Au–Pd NCs with a well-defined octahedral shape. HAADF-STEM-EDS data imply that the prepared NCs are definitely Au–Pd alloys (Figure 3c,d). The ICP-AES-determined composition of the Au–Pd alloy NCs (Au:Pd = 4:1) was the same as that of the Au@Pd core–shell NCs. The surface composition of the Au–Pd alloy NCs was estimated to be Au:Pd = 53:47 by Auger electron spectroscopy, indicating the alloy nature of their surfaces. However, the surface composition is different from the bulk value. This can be attributed to the slower reduction rate of Pd precursor than that of Au precursor.[24] The difference in Pd composition between the bulk and surface of the Au–Pd alloy NCs was also reflected in the change of Pd composition during the reaction (Figure S1 in the Supporting Information).

In the synthesis of the octahedral Au–Pd alloy NCs, the reduction rate is the key to the formation of NCs. In fact, the octahedral Au@Pd core–shell NCs were produced when both metal precursors were co-reduced by cetyltrimethylammonium chloride (CTAC) in the absence of ascorbic acid.[24] Owing to the slow reduction kinetics, the formation of the Au@Pd NCs was initiated by nucleation of Au atoms to form the Au octahedral core, followed by the epitaxial growth of a Pd layer on the Au core. To verify the importance of the reduction rate, we synthesized NCs by employing various amounts of L-ascorbic acid under otherwise identical experimental conditions. When the final concentration of L-ascorbic acid was decreased to 0.05 mM (0.075 mM ascorbic acid was used in the preparation of the Au–Pd alloy NCs shown in Figure 2a), roughly truncated octahedral NCs with an average size of 60 nm were produced in 2 h, which are larger than the Au–Pd alloy NCs (Figure S2 and S3a in the Supporting Information). The compositional line profiles obtained by HAADF-STEM-EDS proved that the prepared NCs with 0.05 mM ascorbic acid for 2 h are Au NCs (Figure S3d). After 24 h reaction time, Au@Pd core–shell NCs with dendritic Pd shell were finally formed (Figure S3b,e). This slow reduction process with 0.05 mM ascorbic acid yielded a small number of Au seeds, and then, a relatively larger amount of the remaining precursors were slowly reduced on the seeds, leading to the formation large Au NCs. Through the subsequent reduction of Pd, Au@Pd core–shell NCs were eventually formed. When a relatively larger amount of L-ascorbic acid (0.1 mM) was used than that used in the original experiment, quasi-spherical NCs with an average size of 20 nm were synthesized (Figure S3c). The compositional line profiles show the formation of alloy NCs (Figure S3f). The formation of smaller alloy NCs can be attributed to the fast reduction rate, which commonly

produces a larger number of seeds. Taken together, the control of the reduction kinetics through the use of an appropriate amount of L-ascorbic acid is crucial to the formation of well-defined octahedral Au–Pd alloy NCs.

High-resolution TEM (HRTEM) images and the corresponding selected-area fast Fourier transform (FFT) patterns of the octahedral NCs are shown in Figure S4 in the Supporting Information. The *d* spacings for adjacent lattice fringes of the Au–Pd alloy, Au@Pd core–shell, Pd, and Au NCs are 2.30, 2.24, 2.24, and 2.36 Å, respectively, which correspond to those of the (111) planes of face-centered cubic (fcc) Au–Pd, Au@Pd, Pd, and Au, respectively (insets of Figure S4a,c,e,g), indicating that the surfaces of all the prepared NCs are bound by {111} facets.[24,26,27] For the Au@Pd core–shell NCs, the lattice distance of the Pd shell region was especially measured. FFT patterns further support that all the octahedral NCs are single crystals enclosed by {111} facets (Figure S4b,d,f,h). The X-ray diffraction (XRD) patterns of the NCs also show the characteristic diffraction peaks from the reflections of the fcc metal structure (Figure S5), demonstrating the crystalline nature of the prepared NCs. For the Au–Pd alloy NCs, XRD peaks were observed between the peak positions for Pd and Au NCs, revealing the formation of single-phase Au–Pd alloy.

To investigate the influence of atomic distribution on the catalytic activity of NCs, the electrocatalytic properties of the NCs for formic acid oxidation were tested. For electrochemical experiments, 2 μg of NCs (based on ICP-AES analysis) were loaded onto a glassy carbon electrode (GCE) for each sample. Since the elimination of surfactants and residual organic materials on the NC surface is very critical for exact catalysis experiments,[28,29] the NC-loaded electrodes were precleaned by potential cycling between 0.25 and 1.0 V at a scan rate of 50 $mV s^{-1}$ until stable cyclic voltammograms (CVs) were obtained. For the Au NCs, potential ranging from 0 to 1.45 V was used for electrochemical cleaning. The CVs of the various NCs in 0.1 M $HClO_4$ are displayed in Figure 4a. In the CVs of the Pd NCs, characteristic current peaks that can be ascribed to the hydrogen adsorption/desorption on Pd-(111) surface are identified around −0.2 and 0 V, indicating the effective removal of surfactants and organic materials from the surfaces of the NCs by the electrochemical cleaning process. The hydrogen adsorption/desorption peaks of the Au–Pd alloy and Au@Pd core–shell NCs were positively shifted relative to those of the Pd NCs. This result can be attributed to the presence of Au on the surface and in the core of NCs for the Au–Pd alloy and Au@Pd core–shell NCs, respectively, which could modify the adsorption/desorption characteristics of Pd for hydrogen. The Au NCs showed no peak associated with hydrogen adsorption/desorption because Au is inactive for hydrogen adsorption.[30] It is noticeable that the oxidative currents of the Au–Pd alloy and Au@Pd core–shell NCs from the formation of surface oxides started at 0.6 V, whereas the onset potential of oxidative current on the Pd NCs was 0.5 V. This finding implies that the incorporation of Au into NCs could improve their resistance to oxidation.

Figure 4b shows the formic acid electrooxidation activities of four different types of octahedral NCs. The CVs were

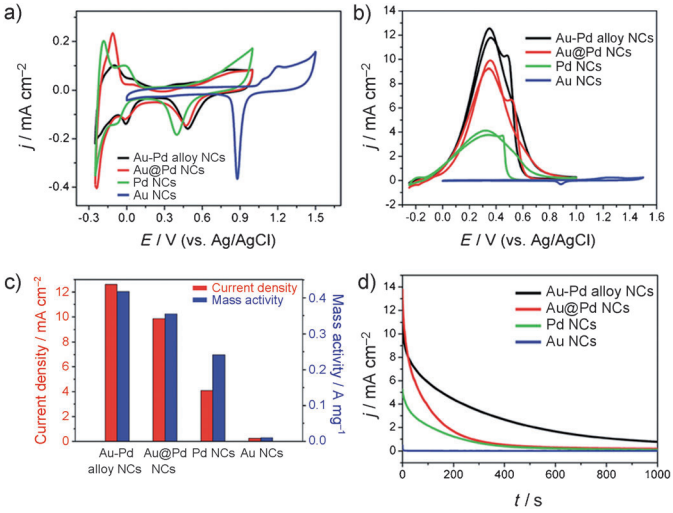

Figure 4. CVs of the Au–Pd alloy, Au@Pd core–shell, Pd, and Au NCs on GCE in a) 0.1 M $HClO_4$ and b) 0.1 M $HClO_4$ + 0.5 M formic acid. Scan rate: 50 $mV s^{-1}$. Current values were normalized with respect to the ECSA. c) Current densities and mass activities for formic acid oxidation on the four different types of NCs. d) Chronoamperometric curves of the NCs on GCE in 0.1 M $HClO_4$ + 0.5 M formic acid at 0.2 V vs. Ag/AgCl. Current values were normalized with respect to the ECSA.

obtained in 0.1 M $HClO_4$ solution containing 0.5 M formic acid, and the current values were normalized to the electrochemically active surface areas (ECSA). The ECSA values were calculated by measuring the coulombic charge for desorption of the monolayer of oxygen.[31,32] As shown in the CV traces, when the electrode potential was scanned from −0.2 to 1.0 V vs. Ag/AgCl, distinct peaks assigned to the oxidation of formic acid through the efficient formate pathway (see below) were observed at about 0.3 V vs. Ag/AgCl on the Au–Pd alloy, Au@Pd, and Pd NCs. Au NCs scarcely exhibited catalytic activity for formic acid oxidation.[33] On the reverse scan, small peaks attributed to the oxidation of adsorbed CO intermediate were observed at 0.6 and 0.5 V vs. Ag/AgCl for Au–Pd NCs and Pd NCs, respectively, were followed by the oxidation of formic acid at similar potentials as those observed in the forward potential sweep. It is noteworthy that the current density of the Au–Pd alloy NCs is highest among the various NCs over the entire potential region. The peak current density of the Au–Pd alloy NCs was 12.3 $mA cm^{-2}$, which is about 1.3 and 3.0 times higher than those of the Au@Pd NCs (9.8 $mA cm^{-2}$) and the Pd NCs (4.1 $mA cm^{-2}$), respectively (Figure 4c). Moreover, the corresponding mass activity of the Au–Pd alloy NCs was 0.42 A/mg_{Au+Pd}, whereas those for the Au@Pd and Pd NCs were 0.35 A/mg_{Au+Pd} and 0.24 A/mg_{Pd}, respectively (Figure 4c). Interestingly, the Au@Pd core–shell NCs showed better electrocatalytic activity than Pd NCs, although the surfaces of the two NCs were composed of the same metal. This result means that the incorporation of Au into the core and the surface of Pd NCs could improve their electrocatalytic performance. Chronoamperometric experiments at 0.2 V vs. Ag/AgCl also reveal that the electrochemical stability of the Au–Pd alloy NCs for formic acid electrooxidation is superior to that of other NCs. The oxidation current on the Au–Pd

alloy NCs at the end of measurement is higher than those on the other NCs, and the current decay is the slowest among the various NCs (Figure 4d). The catalysis experiments unambiguously demonstrate that Au enhances the properties of Pd NCs although it cannot directly oxidize formic acid, and that the atomic distribution in the NCs has a profound influence on the electrocatalytic activities and stabilities of the NCs. The electrocatalytic performances of the four different catalysts follow the order Au–Pd alloy > Au@Pd core–shell > Pd ≫ Au NCs.

It has been widely accepted that formic acid oxidation can proceed by the dual pathway shown in Equations (1) and (2).[34]

reactive intermediate (formate) pathway :

$$HCOOH \rightarrow HCOO_{ads} + H^+ + e^- \rightarrow CO_2 + 2H^+ + e^- \quad (1)$$

poisoning intermediate (CO) pathway :

$$HCOOH \rightarrow CO_{ads} + H_2O \rightarrow CO_2 + 2H^+ + 2e^- \quad (2)$$

Since adsorbed CO generally disturbs formic acid oxidation by blocking catalytically active sites, the formate pathway is a more efficient route than the CO pathway, and it has been reported to be the main pathway for formic acid oxidation on Pd-based catalysts.[35,36] It can be speculated that the formate pathway is more activated on both the Au–Pd alloy and Au@Pd core–shell NCs than on the Pd NCs due to the modification of the electronic structure of Pd by the incorporation of Au. To investigate the change of the electronic structure of Pd in the Au–Pd alloy and Au@Pd core–shell NCs, all NCs were characterized by X-ray photoelectron spectroscopy (XPS). Binding energies for Pd 3d of the Au–Pd alloy and Au@Pd core–shell NCs shifted to lower values than those of the Pd NCs (Figure S6). For example, the Pd $3d_{5/2}$ binding energies of the Au–Pd alloy and Au@Pd core–shell NCs are 335.5 and 335.6 eV, respectively, whereas that of the Pd NCs is 337 eV. This modified electronic structure of Pd in Au–Pd alloy and Au@Pd core–shell NCs can optimize the binding energy between formate ($HCOO_{ads}$) and Pd on the NC surface,[37] thus resulting in enhanced activities toward formic acid oxidation compared to Pd NCs because decomposition of formate to CO_2 is a rate-determining step in the formate pathway.[34]

Although the formate pathway is the efficient main route of formic acid oxidation, the CO pathway is frequently involved together with the formate pathway in formic acid oxidation. Therefore, a practical route to enhance the activity of catalysts for formic acid electrooxidation is to eliminate the adsorbed CO on their surfaces. In this regard, catalysts that can easily oxidize adsorbed CO to CO_2 have shown excellent activity toward formic acid electrooxidation. In several previous reports, CO-stripping experiments were used to evaluate the CO removal ability of NCs.[38,39] Therefore, we performed CO-stripping experiments to check the CO-removal abilities of the NCs. The CO-stripping voltammograms clearly reveal that the Au–Pd alloy NCs are the most effective for CO oxidation (Figure S7). In addition, the Au@Pd core–shell NCs were more efficient than the Pd NCs for CO removal. No CO stripping peak was observed on the Au NCs. The higher CO removal abilities of bimetallic Au–Pd NCs are responsible for the mixing effect of Au with Pd. The incorporation of Au into Pd could induce the improvement of the CO oxidation capability of the bimetallic NCs through the lowering of CO adsorption energy,[40] thus more Pd active sites were available for the formic acid oxidation. From the better CO-removal performance of Au–Pd alloy NCs over Au@Pd NCs, it can be inferred that Au on the surface (Au–Pd alloy NCs) more effectively blocks the adsorption of CO than Au in the core (Au@Pd NCs), thus resulting in the higher electrocatalytic activity and stability of the Au–Pd alloy NCs over the Au@Pd NCs.

In summary, we have investigated the influence of atomic distribution on the catalytic properties of bimetallic NCs toward formic acid electrooxidation. For this study, Au–Pd alloy, Au@Pd core–shell, Pd, and Au NCs with the identical octahedral shape and with similar NC size were prepared to exclusively examine the effect of atomic distribution on the catalytic performance of NCs. The catalytic activities and stabilities are highly dependent on the atomic distribution in the NCs. The overall electrocatalytic performances of the various catalysts follow the order Au–Pd alloy > Au@Pd core–shell > Pd ≫ Au NCs. Au–Pd bimetallic NCs exhibited higher electrocatalytic activity and stability for formic acid oxidation than those of monometallic NCs, and the Au–Pd alloy NCs resulted in the largest improvement in the catalytic activity. The enhanced reactivity of the Au–Pd alloy NCs can be attributed to the modified electronic structure and their excellent CO removal ability due to the promotional effect of Au on the surface of NCs. This method can be extended to other metal systems, and further improvement of catalytic performance and its application to other catalytic reactions are expected through more precise tuning of the morphology and atomic distribution of NCs.

Received: April 14, 2011
Published online: August 2, 2011

Keywords: alloys · electrocatalysis · gold · nanocrystals · palladium

[1] V. R. Stamenkovic, B. Fowler, B. S. Mun, G. Wang, P. N. Ross, C. A. Lucas, N. M. Markovic, *Science* **2007**, *315*, 493.
[2] B. Lim, M. Jiang, P. H. C. Camargo, E. C. Cho, J. Tao, X. Lu, Y. Zhu, Y. Xia, *Science* **2009**, *324*, 1302.
[3] J. Greeley, I. E. L. Stephens, A. S. Bondarenko, T. P. Johansson, H. A. Hansen, T. F. Jaramillo, J. Rossmeisl, I. Chorkendorff, J. K. Nørskov, *Nat. Chem.* **2009**, *1*, 552.
[4] Y. Kim, J. W. Hong, Y. W. Lee, M. Kim, D. Kim, W. S. Yun, S. W. Han, *Angew. Chem. Int. Ed.* **2010**, *49*, 10197.
[5] M. A. Mahmoud, F. Saira, M. A. El-Sayed, *Nano Lett.* **2010**, *10*, 3764.
[6] S. Habas, H. Lee, V. Radmilovic, G. A. Somorjai, P. Yang, *Nat. Mater.* **2007**, *6*, 692.
[7] Y. Yu, Q. Zhang, B. Liu, J. Y. Lee, *J. Am. Chem. Soc.* **2010**, *132*, 18258.
[8] C.-L. Lu, K. S. Prasad, H.-L. Wu, J. A. Ho, M. H. Huang, *J. Am. Chem. Soc.* **2010**, *132*, 14546.
[9] J. Wu, A. Gross, H. Yang, *Nano Lett.* **2011**, *11*, 798.

[10] Y. Lei, F. Mehmood, S. Lee, J. Greeley, B. Lee, S. Seifert, R. E. Winans, J. W. Elam, R. J. Meyer, P. C. Redfern, D. Teschner, R. Schlögl, M. J. Pellin, L. A. Curtiss, S. Vajda, *Science* **2010**, *328*, 224.

[11] W. P. Zhou, A. Lewera, R. Larsen, R. I. Masel, P. S. Bagus, A. Wieckowski, *J. Phys. Chem. B* **2006**, *110*, 13393.

[12] S. H. Joo, J. Y. Park, J. R. Renzas, D. R. Butcher, W. Huang, G. A. Somorjai, *Nano Lett.* **2010**, *10*, 2709.

[13] D. Wang, H. L. Xin, Y. Yu, H. Wang, E. Rus, D. A. Muller, H. D. Abruña, *J. Am. Chem. Soc.* **2010**, *132*, 17664.

[14] J. Zhang, H. Yang, J. Fang, S. Zou, *Nano Lett.* **2010**, *10*, 638.

[15] V. Mazumder, M. Chi, K. L. More, S. Sun, *J. Am. Chem. Soc.* **2010**, *132*, 7848.

[16] S. T. Marshall, M. O'Brien, B. Oetter, A. Corpuz, R. M. Richards, D. K. Schwartz, J. W. Medlin, *Nat. Mater.* **2010**, *9*, 853.

[17] J. Snyder, T. Fujita, M. W. Chen, J. Erlebacher, *Nat. Mater.* **2010**, *9*, 904.

[18] H. Lee, S. E. Habas, G. A. Somorjai, P. Yang, *J. Am. Chem. Soc.* **2008**, *130*, 5406.

[19] J.-Y. Wang, Y.-Y. Kang, H. Yang, W.-B. Cai, *J. Phys. Chem. C* **2009**, *113*, 8366.

[20] X. Huang, S. Tang, X. Mu, Y. Dai, G. Chen, Z. Zhou, F. Ruan, Z. Yang, N. Zheng, *Nat. Nanotechnol.* **2011**, *6*, 28.

[21] Y. W. Lee, M. Kim, S. W. Han, *Chem. Commun.* **2010**, *46*, 1535.

[22] V. Mazumder, S. Sun, *J. Am. Chem. Soc.* **2009**, *131*, 4588.

[23] M. Baldauf, D. M. Kolb, *J. Phys. Chem.* **1996**, *100*, 11375.

[24] Y. W. Lee, M. Kim, Z. H. Kim, S. W. Han, *J. Am. Chem. Soc.* **2009**, *131*, 17036.

[25] D. Kim, J. Heo, M. Kim, Y. W. Lee, S. W. Han, *Chem. Phys. Lett.* **2009**, *468*, 245.

[26] J. W. Hong, Y. W. Lee, M. Kim, S. W. Kang, S. W. Han, *Chem. Commun.* **2011**, *47*, 2553.

[27] Y. W. Lee, N. H. Kim, K. Y. Lee, K. Kwon, M. Kim, S. W. Han, *J. Phys. Chem. C* **2008**, *112*, 6717.

[28] J. Wu, J. Zhang, Z. Peng, S. Yang, F. T. Wagner, H. Yang, *J. Am. Chem. Soc.* **2010**, *132*, 4984.

[29] H. Yang, J. Zhang, K. Sun, S. Zou, J. Fang, *Angew. Chem. Int. Ed.* **2010**, *49*, 6848.

[30] S. Zhang, Y. Shao, G. Yin, Y. Lin, *Angew. Chem. Int. Ed.* **2010**, *49*, 2211.

[31] The ECSA value was calculated by the following equation: $ECSA = Q_o/q_o$, where Q_o is the surface charge obtained from the area under the CV trace of oxygen desorption and q_o is the charge required for desorption of monolayer of oxygen on the NC surfaces (411, 424, 424, and 400 $\mu C\,cm^{-2}$ for the Au–Pd, Au@Pd, Pd, and Au NCs, respectively).[32]

[32] R. Woods in *Electroanalytical Chemistry: A Series of Advances*, *Vol. 9* (Ed.: A. J. Bard), Marcel Dekker, New York, **1974**, pp. 1 – 162.

[33] D. Zhao, Y.-H. Wang, B.-Q. Xu, *J. Phys. Chem. C* **2009**, *113*, 20903.

[34] M. Osawa, K.-I. Komatsu, G. Samjeské, T. Uchida, T. Ikeshoji, A. Cuesta, C. Gutiérrez, *Angew. Chem.* **2011**, *123*, 1191; *Angew. Chem. Int. Ed.* **2011**, *50*, 1159.

[35] F. J. Vidal-Iglesias, J. Solla-Gullón, E. Herrero, A. Aldaz, J. M. Feliu, *Angew. Chem. Int. Ed.* **2010**, *49*, 6998.

[36] Y. Lu, W. Chen, *J. Phys. Chem. C* **2010**, *114*, 21190.

[37] K. Tedsree, C. W. A. Chan, S. Jones, Q. Cuan, W.-K. Li, X.-Q. Gong, S. C. E. Tsang, *Science* **2011**, *332*, 224.

[38] J. L. Haan, K. M. Stafford, R. I. Masel, *J. Phys. Chem. C* **2010**, *114*, 11665.

[39] J. Zhang, C. Qiu, H. Ma, X. Liu, *J. Phys. Chem. C* **2008**, *112*, 13970.

[40] X. Hao, B. Shan, J. Hyun, N. Kapur, K. Fujdala, T. Truex, K. Cho, *Top. Catal.* **2009**, *52*, 1946.

